



Published in final edited form as:

Environ Sci Technol. 2009 August 15; 43(16): 6349–6356.

Toxicity and developmental defects of different sizes and shape nickel nanoparticles in zebrafish

Cristina Ispas^{1,2}, Daniel Andreescu^{1,2}, Avni Patel³, Dan V. Goia^{1,2}, Silvana Andreescu^{1,2,*}, and Kenneth N. Wallace^{1,3,*}

¹ Department of Chemistry and Biomolecular Science, Clarkson University, Potsdam, NY 13699-5810, USA

² Center for Advanced Materials Processing (CAMP), Clarkson University, Potsdam, NY 13699-5810, USA

³ Department of Biology, Clarkson University, Potsdam, NY 13699-5810, USA

Abstract

Metallic nanoparticles such as nickel are used in catalytic, sensing and electronic applications, but health and environmental effects have not been fully investigated. While some metal nanoparticles result in toxicity, it is also important to determine whether nanoparticles of the same metal but of different size and shape changes toxicity. Three different size nickel nanoparticle (Ni NPs) of 30, 60, and 100 nm and larger particle clusters of aggregated 60 nm entities with a dendritic structure were synthesized and exposed to zebrafish embryos assessing mortality and developmental defects. Ni NPs exposure was compared to soluble nickel salts. All three 30, 60, and 100 nm Ni NPs are equal to or less toxic than soluble nickel while dendritic clusters were more toxic. With each Ni NP exposure, thinning of the intestinal epithelium first occurs around the LD10 continuing into the LD50. LD50 exposure also results in skeletal muscle fiber separation. Exposure to soluble nickel does not cause intestinal defects while skeletal muscle separation occurs at concentrations well over LD50. These results suggest that configuration of nanoparticles may affect toxicity more than size and defects from Ni NPs exposure occur by different biological mechanisms than soluble nickel.

Keywords

nickel; nanoparticles; nanotoxicity; zebrafish; size effect; shape effect; digestive; intestine; accumulation and organ defects; cytotoxicity

INTRODUCTION

Nanoparticles (NPs) and nanostructures are materials with dimensions at or below 100 nm, creating unique properties, different from the bulk materials (1–3). While many nanomaterials are commonly used, their interactions with biological systems as well as their environmental and health effects are largely unknown (4–7). Nanostructures show varying degrees of toxic effects in living organisms, which are not observed with larger particles or bulk material (8, 9).

*Corresponding authors: eandrees@clarkson.edu, kwallace@clarkson.edu.

Supporting Information Available

Aggregation of Ni NPs in the growth medium (Figure S1). This information is available free of charge via the Internet at <http://pubs.acs.org/>

Organisms are exposed to environmental sources of nanoparticles through the skin, digestive system, and respiratory tract (10). Studies have focused on assessment of health effects of NPs exposure by respiratory, gastrointestinal, dermal, injection of mice (11,12), and cell culture (8,13,14). While skin functions as a barrier to the environment, the respiratory and digestive tract are designed to absorb gasses and nutrients across the luminal surface. Internalized nanoparticles can result in extended exposure depending on nanoparticle retention. Differences in nanoparticle size and shape may change retention time, increasing or decreasing toxic effects. Many mechanisms of translocation, accumulation, and retention pathways in organs are unknown and need further study (3,15).

Zebrafish is an attractive model system to study affects of environmental exposure to nanoparticles. Zebrafish can be used as a test organism for affects of environmental release of nanoparticles both on aquatic and terrestrial vertebrates due to similarities in development and cellular composition of major organ systems (16–18). Similarities in organ physiology between zebrafish and other vertebrates also make this a good model system to identify potential health affects in humans. During embryogenesis, their small size, rapid development, optical clarity, ease of care, and ability to obtain large numbers (19), make zebrafish an attractive model for rapid screening of developmental and toxicological effects from nanoparticle exposure.

To investigate differences in mortality and development due to size and shape of nanoparticles using zebrafish, we choose a metal with intermediate toxicity. Numerous studies describe the toxicity of soluble Ni (e.g. NiCl_2 , NiSO_4) (20–22). However, little is known about cytotoxic effects or developmental defects with nanometer size nickel (15,23,24). The objective of this study was to determine whether size and shape of Ni NPs alters the level of toxicity and the type of developmental defects during zebrafish embryogenesis. To this end, three different size sphere NPs (30, 60 and 100 nm) and one structure consisting of aggregated 60 nm particles (dendritic) were used to identify toxicity levels. Embryos were exposed to Ni NPs during the last four days of embryogenesis to identify the range of developmental defects that can occur. Each of these Ni NPs is synthesized in a similar manner and is essentially of the same composition. Histological analysis identifies major defects within the digestive system, suggesting this to be a major route of exposure during embryogenesis. Exposure of different size NPs and shape was also compared with bulk nickel to determine the role of soluble nickel in the toxicity of NPs exposure.

MATERIALS AND METHODS

Reagents and Instrumentation

Ni particles were synthesized in the Center for Advanced Materials Processing at Clarkson University using established procedures via the polyol process, starting from nickel carbonate (Shepherd Chemical Co., Norwood, OH) and Pt as a catalyst (25–28). 1,2-Propylene glycol (PG), diethylene glycol (DEG) and ethyl alcohol were obtained from Alfa Aesar (Ward Hill, MA). Triethanolamine (TEA) was purchased from Aldrich (Milwaukee, WI). Bis (ethanolamine)hexahydroxoplatinate – $(\text{EA})_2\text{Pt}(\text{OH})_6$ – (9%) solutions were provided by OMG. Metal salts were reduced by boiling the polyol from 3 to 12 hours. After reduction was completed, the Ni particles were first washed with deionized water and ethanol, filtered and dried at 100°C for 10 hours.

Electrokinetic properties and zeta potential (ζ -potential) were measured with a Brookhaven Zeta Plus – Zeta Potential Analyzer at 25°C and calculated with standard software. pH adjustments were made with HCl and NaOH 10^{-2} M as necessary. Ionic strength was adjusted with a common electrolyte (KCl). Size and morphology of spheres and dendritic particles were measured with a JEOL JSM-7400F high resolution field emission scanning electron microscope. Specific surface area (SSA) of the dry nickel powders was measured with a

Brunauer–Emmet–Teller (BET) method using a Quantachrome Nova (Boyton Beach, FL) 1200e. Particle size distribution (PSD) was calculated with dispersion technology software from FESEM images (average values of 100 particles) and by laser diffraction using a Malvern Mastersizer 2000. Soluble nickel was measured with a Thermo Electron X7 ICP-MS system. E3 embryo medium consisting of 5 mM NaCl, 0.17 mM KCl, 0.33 mM CaCl₂, 0.33 mM MgSO₄ was used in all exposures. Nickel nanoparticles were incubated with E3 embryo media in metal free plates and handled with metal free tips. E3 was filtered using 5,000 NMWL Amicon Ultrafree-MC filters (Millipore) to remove any remaining Ni NPs suspensions. For comparison, embryos were exposed to 1000 mg/L of 25 nm cerium oxide NPs, which are considered biocompatible and FDA approved. E3 incubated without Ni NPs were used as controls.

Fish stocks

Fish are maintained in an Aquatic Habitat recirculating tank system at 28.5°C with 14 hrs light/ 10 hrs dark. Water is purified by reverse osmosis and adjusted to pH 7 with conductivity of 350 µS. Embryos are collected in E3 and divided into 50 per Petri dish. AB fish stock used in all procedures originated from the Oregon Stock center (19).

Nanoparticle exposure

24 hpf embryos are manually dechorionated. NP powder was suspended in E3 at specific amounts between 10 to 1000 mg/L and sonicated for at least ½ h. 5 mL of suspended NPs and 25 embryos (after dechoriation) are added to 6 well plates. Embryos were grown to 5 dpf and lethality was assessed by lack of heartbeat. Surviving embryos were fixed in 4% formaldehyde for 2 h to overnight and assayed by immunohistochemistry, alcian blue staining, or histology for developmental defects. At least three replicates were done for each size, shape, and concentration. LD10 and LD50 were calculated by the Hill method using the REGTOX macro in Microsoft Excel.

For animal loading experiments, embryos were exposed to NP concentrations at the LD50. Groups of five embryos were digested in 70% nitric acid (Optima grade, Fisher Scientific) and 30% hydrogen peroxide (Mallinckrodt Baker) using CEM-Mars 5 express. Digestions were filtered and incorporated nickel was measured by ICP-MS.

Immunohistochemistry

Fixed embryos were permeabilized with Proteinase K (Sigma) in PBS for 20 minutes at room temperature and incubated at 4°C overnight with primary antibody (mouse anti-collagen, 1:100, Developmental Studies Hybridoma Bank). Embryos were washed and incubated with secondary antibody (Alexa Fluor 488 conjugated anti-mouse Ig, 1:500) (Molecular Probes - Invitrogen). Fluorescent imaging was performed on a Nikon Eclipse TE2000 inverted compound microscope.

Alcian Blue staining and embryo visualization

Embryos were stained overnight in 0.1 mg/ml Alcian Blue/80% ethanol/20% glacial acetic acid and washed in 10% glacial acetic acid/90% ethanol and rehydrated in PBST. Embryos are digested in 25 mg/ml trypsin/60% sodium tetraborate and cleared in glycerol. Embryos were analyzed by whole mount or processed for histology by infiltration and embedding in glycol methacrylate (JB4 plus; Polysciences). Five micron sections were cut on a Lecia RM2135 and stained in methylene blue/azure II (29). Whole mount and sectioned embryos were analyzed on an Olympus BH2.

RESULTS

Physico-chemical characterization of nickel nanoparticles

Particles were obtained by reduction of nickel carbonate, followed by precipitation in liquid polyols, (26,27) using a well established synthetic method to prepare metal NPs. Here, the polyol acts as both as a solvent and reducing agent (25). NPs were characterized by size, shape, surface area, particle size distribution, charge and solubility, as summarized in Table 1. To determine whether different size and shape NPs induce different defects, we have studied Ni NPs of 30, 60 and 100 nm diameter and a dendritic structure, with aggregated 60 nm entities. SEM images show that all particles have nearly uniform size and are well dispersed (Figure 1). After exposure in E3, NPs form visible aggregates (Figure S1, Supporting Information). XRD patterns (Figure 2A) of resulting particles reveal characteristic peaks of pure face centered cubic (*fcc*) for nickel (JCPDS, No. 04–0850). Figure 2B shows zeta-potential analysis of the four types of particles. 100 nm and dendritic particles have a positive charge over the entire pH range while the charge of 30 and 60 nm NPs shifts from positive to negative at pH value of ~8.5. Change in zeta-potential can be attributed to increased reactivity of smaller size particles and possible formation of a nickel oxide layer. Particle size distribution (PSD) was several times higher for dendritic Ni, which has multiple 60 nm nano-sized particles on the surface (Figure 2C).

We studied dissolution of Ni NPs in E3 medium to estimate the contribution of dissolved nickel ions to overall cytotoxic effects. Concentration of soluble nickel in E3 after NPs exposure was measured using inductively coupled plasma mass spectroscopy (ICP-MS) after ultrafiltration to remove suspended metallic particles. A concentration of 1000 mg/L Ni NPs powder was incubated with the embryo medium for 4 days at 28.5°C. The concentration for ICP-MS analysis was the highest used in the cytotoxicity studies and these concentrations can be considered maximum values during these experiments. Results from ICP-MS analysis indicate that there is a small amount of soluble nickel produced by dissolution of NPs in E3.

Exposure of Ni NPs to zebrafish embryo

Zebrafish embryos were exposed to Ni NPs of different sizes and shapes to determine levels of toxicity, identify the site of NPs accumulation, and study development defects. NPs as well as soluble Ni were introduced to E3 after dechoriation at 24 hours post fertilization (hpf) and left with the embryos until 5 days post fertilization (dpf), corresponding to the end of embryogenesis. Surviving embryos were fixed for analysis. We choose this period for exposure to avoid early development (including axis formation) but instead expose embryos during a time when many of the major organs are developing. The digestive system undergoes dramatic changes and opens to the outside environment during later embryogenesis.

During embryogenesis, embryos do not move through the water column and mostly remain on the substrate until the swim bladder is inflated late in the fourth day. As a result, embryos are not only exposed to suspended NPs but are also exposed to NPs undergoing aggregation and sedimentation. Range finding experiments identified concentrations of 1000 mg/L as the upper limit, resulting in near 100 % mortality. Equally spaced doses below 1000 mg/L identified LD10 and LD50s for each size and shape of the Ni NPs. Embryos were exposed to 30, 60, and 100 nm NPs as well as larger dendritic Ni structures. Dose-response curves for each of the NPs are plotted in comparison to soluble Ni (Figure 3). Embryos were also exposed to 1000 mg/L of 25 nm cerium oxide NPs for comparison as well as groups with no NPs as controls.

Calculation of both LD10 and LD50 values reveals a higher level of toxicity for the dendritic Ni than for any of the other sizes. The toxicity of 30, 60 and 100 nm Ni NPs results in similar LD10 and LD50 values and overlapping 95% confidence intervals (Table 2). In contrast,

toxicity of dendritic clusters is higher than toxicity of soluble Ni. Even though the 95% confidence interval has some overlap at the LD10 for the dendritic structures and the soluble Ni, the calculated LD10 and LD50 values are lower for the dendritic particles, suggesting a higher toxicity than soluble Ni. In contrast, exposure to cerium oxide NPs does not increase mortality above populations of embryos with no NPs.

Accumulation of NPs in the digestive tract lumen

Presence of NP aggregates of each size and shape are observed within the digestive system lumen but location varies between embryos. In some exposures, large aggregations are visible in the pharynx and intestine when viewed in whole mount (Figure 4B). Embryos exposed to Ni NPs and cross sectioned along the anterior to posterior axis have NPs aggregates that vary between smaller groups of particles to larger accumulations filling a large percentage of the lumen. Figure 4D is an example showing the presence of 100 nm particles at 100 mg/L and Figure 4E is an example of dendritic clusters at 20 mg/L. Variable accumulation of NPs within the digestive system may result in variable exposure of epithelial cells, explaining variation in the dose-response curves.

Initial studies of animal loading reveals a higher level of nickel per embryo with 60 nm Ni spheres when compared to dendritic particles. Digestion of exposed embryos followed by ICPMS analysis demonstrates an average level of nickel to be 7.97 ng/embryo (n=4; SD=3.76) with sphere exposure. In contrast, the average level of nickel in dendritic exposures is 1.69 ng/embryo (n=4; SD=1.29). This suggests that there are lower numbers of dendritic particles incorporated into embryos than 60 nm Ni NP spheres.

Comparison between metallic NPs and soluble nickel on embryos

Defects were analyzed in embryos exposed to each size and shape of Ni NPs suspensions as well as an equivalent mass of soluble Ni. While NP exposed embryos have more yolk at 5 dpf than unexposed embryos (Figure 4A and 4B), development of the digestive system is comparable between the two groups (Figure 4C to 4E). Anterior to posterior cross-sections reveal intestinal defects only in embryos exposed to NPs while skeletal muscle defects are observed in both NP and soluble Ni exposure.

By the fifth day of embryogenesis, intestinal epithelial cells become columnar and the intestine has numerous folds (anterior- Figure 5A and posterior- Figure 5B). At the lower end of the dose-response curve, NP exposure reveals embryos with under-developed intestinal epithelial cells around the LD10 values. Epithelial cells are cuboidal and there is very little folding within the intestine (anterior- Figure 5C and posterior- Figure 5D). One exception is the 60 nm particles, which begin to show intestinal defects at concentrations lower than the LD10 (at 50 mg/L with the LD10 at 189 mg/L). As the concentration of NPs increases, defects continue to be observed in intestinal epithelial cells. At the LD50, intestinal epithelial cells continue to be cuboidal with little folding, similar to what is observed at the LD10, but here the trunk skeletal muscle fibers are also separated along the anterior to posterior axis (anterior- Figure 5E and posterior- Figure 5F). Exposure to 25 nm cerium oxide NPs at 1000 mg/L does not result in intestinal or skeletal muscle defects.

While toxicity levels of soluble Ni are similar to the NPs, soluble Ni exposure does not share similar defects with NPs exposure. At both the LD10 and LD50 values, soluble Ni exposure does not display intestinal or skeletal muscle defects. Skeletal muscle defects only occur at much higher concentrations above the LD50 (221 mg/L) with separation of skeletal muscle fibers first seen at 800 mg/L (anterior- Figure 5G and posterior Figure 5H). Unlike Ni NP exposure, intestinal epithelial cells become columnar with normal intestinal folding even at Ni concentrations causing skeletal muscle separation (arrows in 5G and 5H). Soluble Ni appears

to result in toxicity through a different route than the NPs due lack of both intestinal and skeletal defects in soluble Ni exposure at LD10 and LD50 values. This suggests that NP defects are due to the presence of the particles and not the presence of dissolved Ni from these NPs.

Jaw patterning is defective in embryos exposed to nickel nanoparticles

Ni NP exposure also results in defects in head and jaw cartilage becoming more frequent and severe with increasing NPs concentrations. Defects in development of the head skeleton were identified by both alcian blue staining and collagen immunohistochemistry. Cartilage defects are seen with concentrations approaching the LD50. The lower jaw develops altered spacing between Meckel's and ceratohyal cartilage (Figure 6).

DISCUSSION

The results demonstrate that shape of Ni NPs have dramatic differences in toxicity upon exposure to zebrafish embryos. Different diameter spherical Ni NPs results in similar levels of toxicity to zebrafish embryos. However, exposure to dendritic clusters consisting of aggregated 60 nm particles results in higher toxicity, suggesting that difference in shape and aggregation is responsible for increased toxicity as synthesis and composition are similar. Higher dendritic aggregate toxicity is apparent at both the LD10 and LD50. Previous studies demonstrate similar dose response toxicity of zebrafish embryos and adults to a variety of other metallic NPs (15,30–34) and C60 (35,36). While changes in toxicity of zebrafish embryos have been observed with differently functionalized C60 (36), this is the first observation of differing toxicities in zebrafish due to metal NPs shape.

Even though toxicity varies between the spherical and dendritic structures, all NPs exposures result in common organ defects correlated with both the LD10 and the LD50. Histological observation of embryos exposed to Ni NPs distinguishes low concentration effects at the LD10 with additional effects at LD50 concentrations. In contrast, embryos exposed to soluble Ni do not develop visible organ defects at the LD10 or LD50, suggesting a different route for toxicity.

Embryos exposed to Ni NPs first develop defects in the intestine with minimal folding and thin cuboidal epithelial cells beginning at LD10 concentrations. Normally by the fifth day of embryogenesis, the intestine is highly folded and epithelial cells are columnar (37,38). These intestinal defects are not immediately lethal because embryos survive on yolk throughout embryogenesis and do not require a functional digestive system. More immediate lethality may occur from secondary defects that occur around LD50 concentrations when skeletal muscle fibers begin to separate in addition to the intestinal defects.

Intestinal epithelial defects with both 60 nm particles and 60 nm dendritic aggregates occur at lower concentrations than the 30 and 100 nm NPs. This suggests that exposure to 60 nm Ni NPs results in more damage or stress to epithelial cells than smaller and larger Ni NPs. One hypothesis for these differences is that 60 nm Ni NPs may more frequently become trapped within luminal spaces and be retained within the intestine for longer periods. Differential retention in kidneys has been observed due to size and shape of NPs after intravenous injection. Small spherical NPs are cleared from the rat kidney however, larger NPs are not excreted (39). It was reported that aggregated carbon nanotubes of different shapes can become trapped in the glomerular capillary (40). Long-term exposure of Ni NPs may stress epithelial cells causing retarded epithelial development and lack of epithelial differentiation may allow particles to pass through intestinal barriers entering other tissues to cause additional defects. Crossing of cell membranes has been observed in zebrafish embryos exposed to silver nanoparticles (30,33) and may occur more frequently when the intestine is compromised.

While intestinal defects occur at lower concentrations in both 60 nm spherical and dendritic NPs, dendritic particles are more toxic than spheres, suggesting that configuration of a particular size NP causes the difference. Also, preliminary animal loading data suggest that average amounts of dendritic aggregates within embryos are lower than 60 nm spheres. Toxicity of dendritic aggregates would then occur at lower doses than 60 nm spheres. We hypothesize that arrangement of particles into an aggregate such as 60 nm dendritic Ni clusters may more readily adhere and be retained for longer periods in the intestinal lumen than individual 60 nm particles.

Internalization of NPs is likely to be an important factor in toxicity and defects generated by NPs with intermediate toxicity such as nickel. Higher concentrations needed to produce the LD50 as compared to other acutely toxic metal NPs (41) (15) are likely to occur less frequently from environmental sources. Defects and lethality due to NPs of intermediate toxicity are more likely linked to accumulation within organs rather than short-term exposures. As a result, environmental release of the same concentration of similar composition NPs of different sizes and shapes may result in different toxicities due to different levels of tissue accumulation.

A portion of the toxicity produced by Ni NPs exposure may also be due to dissolution of nickel within the E3. Variable dissolution rates have been reported for metallic NPs including silver, copper, aluminum, nickel, and cobalt (15,31,32) with a portion of observed toxicity attributed to soluble metal. We observe similar rates of solubilized Ni, from each different size Ni NPs, contributing about 2.4 to 3.8 % of observed toxicity, depending on the size and shape of the particle leaving a significant portion of the observed toxicity resulting from the presence of NPs.

Remaining toxicity can be attributed to colloidal NPs due to the dramatic differences in organ defects observed between particles and soluble nickel exposure. In contrast to common organ defects with exposure to each NP size and shape, soluble Ni does not produce any obvious digestive or skeletal muscle defects until well past the LD50. Skeletal defects only appear after exposure to high concentrations of soluble nickel suggesting different routes for toxicity than observed for NPs. Distinct differences in organ defects between the two forms of nickel suggest that the majority of Ni NPs toxicity is directly related to the presence of particles, and toxicity appears to occur by different mechanisms. Differences between NP exposure and corresponding soluble ions were also observed with copper in gills of adult zebrafish (31,32).

We hypothesize that with higher NPs concentrations, more particles accumulate in the intestine. More NPs would then cover larger areas of the epithelium, allowing particles to begin passing through the intestinal barrier to affect other embryonic tissues. Additional investigation will determine the route of entry and quantity of NPs within exposed embryos.

Supplementary Material

Refer to Web version on PubMed Central for supplementary material.

Acknowledgments

This work was supported in part by grants NSF-0804506 to SA, NIH- 1R15DK074416-01A1 to KW.

References

1. Hood E. Nanotechnology: Looking as we leap. *Environmental Health Perspectives* 2004;112 (13):A740–A749. [PubMed: 15345364]
2. Nel A, Xia T, Madler L, Li N. Toxic potential of materials at the nanolevel. *Science* 2006;311(5761): 622–627. [PubMed: 16456071]

3. Oberdorster G, Oberdorster E, Oberdorster J. Nanotoxicology: An emerging discipline evolving from studies of ultrafine particles. *Environmental Health Perspectives* 2005;113(7):823–839. [PubMed: 16002369]
4. Borm PJA, Robbins D, Haubold S, Kuhlbusch T, Fissan H, Donaldson K, Schins R, Stone V, Kreyling W, Lademann J, et al. The potential risks of nanomaterials: a review carried out for ECETOC. *Particle and Fibre Toxicology* 2006;3–11. [PubMed: 16438714]
5. Englert BC. Nanomaterials and the environment: uses, methods and measurement. *Journal of Environmental Monitoring* 2007;9(11):1154–1161. [PubMed: 17968441]
6. Gwinn MR, Vallyathan V. Nanoparticles: Health effects - Pros and cons. *Environmental Health Perspectives* 2006;114(12):1818–1825. [PubMed: 17185269]
7. Lewinski N, Colvin V, Drezek R. Cytotoxicity of nanoparticles. *Small* 2008;4(1):26–49. [PubMed: 18165959]
8. Elder A, Yang H, Gwiazda R, Teng X, Thurston S, He H, Oberdorster G. Testing nanomaterials of unknown toxicity: An example based on platinum nanoparticles of different shapes. *Advanced Materials* 2007;19(20):3124.
9. Franklin NM, Rogers NJ, Apte SC, Batley GE, Gadd GE, Casey PS. Comparative toxicity of nanoparticulate ZnO, bulk ZnO, and ZnCl₂ to a freshwater microalga (*Pseudokirchneriella subcapitata*): The importance of particle solubility. *Environmental Science & Technology* 2007;41(24):8484–8490. [PubMed: 18200883]
10. Hoet P, Bruske-Hohlfeld I, Salata O. Nanoparticles - known and unknown health risks. *Journal of Nanobiotechnology* 2004;2(1):12. [PubMed: 15588280]
11. Chen Z, Meng HA, Xing GM, Chen CY, Zhao YL, Jia GA, Wang TC, Yuan H, Ye C, Zhao F, et al. Acute toxicological effects of copper nanoparticles in vivo. *Toxicology Letters* 2006;163(2):109–120. [PubMed: 16289865]
12. Meng H, Chen Z, Xing GM, Yuan H, Chen CY, Zhao F, Zhang CC, Zhao YL. Ultrahigh reactivity provokes nanotoxicity: Explanation of oral toxicity of nano-copper particles. *Toxicology Letters* 2007;175(1–3):102–110. [PubMed: 18024012]
13. Brunner TJ, Wick P, Manser P, Spohn P, Grass RN, Limbach LK, Bruinink A, Stark WJ. In vitro cytotoxicity of oxide nanoparticles: Comparison to asbestos, silica, and the effect of particle solubility. *Environmental Science & Technology* 2006;40(14):4374–4381. [PubMed: 16903273]
14. Khan JA, Pillai B, Das TK, Singh Y, Maiti S. Molecular effects of uptake of gold nanoparticles in HeLa cells. *Chembiochem* 2007;8(11):1237–1240. [PubMed: 17569092]
15. Griffitt RJ, Luo J, Gao J, Bonzongo JC, Barber DS. Effect of particle composition and species on toxicity of metallic nanomaterials in aquatic organisms. *Environ Toxicol Chem* 2008;27:1972–1978. [PubMed: 18690762]
16. Schoenebeck JJ, Yelon D. Illuminating cardiac development: Advances in imaging add new dimensions to the utility of zebrafish genetics. *Seminars in Cell & Developmental Biology* 2007;18(1):27–35. [PubMed: 17241801]
17. Rubin DC. Intestinal morphogenesis. *Current Opinion in Gastroenterology* 2007;23(2):111–114. [PubMed: 17268237]
18. Drummond IA. Kidney development and disease in the zebrafish. *Journal of the American Society of Nephrology* 2005;16(2):299–304. [PubMed: 15647335]
19. Westerfield, M. *The zebrafish book: a guide for the laboratory use of zebrafish (Brachydanio rerio)*. University of Oregon Press; Eugene, OR: 1993.
20. Fort DJ, Rogers RL, Thomas JH, Hopkins WA, Schlekot C. Comparative developmental toxicity of nickel to *Gastrophryne carolinensis*, *Bufo terrestris*, and *Xenopus laevis*. *Archives of Environmental Contamination and Toxicology* 2006;51(4):703–710. [PubMed: 16998636]
21. Hoang TC, Tomasso JR, Klaine SJ. Influence of water quality and age on nickel toxicity to fathead minnows (*Pimephales promelas*). *Environmental Toxicology and Chemistry* 2004;23(1):86–92. [PubMed: 14768871]
22. Kienle C, Kohler HR, Filser J, Gerhardt A. Effects of nickel chloride and oxygen depletion on behaviour and vitality of zebrafish (*Danio rerio*, Hamilton, 1822) (Pisces, Cypriniformes) embryos and larvae. *Environmental Pollution* 2008;152(3):612–620. [PubMed: 17720287]

23. Guo DD, Wu CH, Li XM, Jiang H, Wang XM, Chen BA. In vitro cellular uptake and cytotoxic effect of functionalized nickel nanoparticles on leukemia cancer cells. *Journal of Nanoscience and Nanotechnology* 2008;8(5):2301–2307. [PubMed: 18572641]
24. Yin H, Too HP, Chow GM. The effects of particle size and surface coating on the cytotoxicity of nickel ferrite. *Biomaterials* 2005;26(29):5818–5826. [PubMed: 15949547]
25. Fievet F, Lagier JP, Figlarz M. Preparing monodisperse metal powders in micrometer and submicrometer sizes by the polyol process. *MRS Bulletin* 1989:29–34.
26. Goia, DV.; Andreescu, D.; Farrell, BP. Polyol – based method for producing ultra – fine nickel powders. 2006.
27. Goia, DV.; Andreescu, D.; Farrell, BP. Polyol – based method for producing ultra – fine metal powders. 2006.
28. Andreescu, D.; Farrell, BP.; Halaciuga, I.; Laplante, S.; Goia, DV. Preparation of uniform nano and micro copper and nickel powders for electronic applications. *PowderMet: Las Vegas, NV*; 2009.
29. Humphrey CD, Pittman FE. A simple methylene blue-azure II- basic fuchsin stain for epoxy-embedded tissue sections. *Stain Technology* 1974;49(1):9–14. [PubMed: 4131626]
30. AshaRani PV, Mun GLK, Hande MP, Valiyaveetil S. Cytotoxicity and Genotoxicity of Silver Nanoparticles in Human Cells. *ACS Nano* 2009;3(2):279–290. [PubMed: 19236062]
31. Griffitt RJ, Hyndman K, Denslow ND, Barber DS. Comparison of Molecular and Histological Changes in Zebrafish Gills Exposed to Metallic Nanoparticles. *Toxicological Sciences* 2009;107(2):404–415. [PubMed: 19073994]
32. Griffitt RJ, Weil R, Hyndman KA, Denslow ND, Powers K, Taylor D, Barber DS. Exposure to copper nanoparticles causes gill injury and acute lethality in zebrafish (*Danio rerio*). *Environmental Science & Technology* 2007;41(23):8178–8186. [PubMed: 18186356]
33. Lee KJ, Nallathamby PD, Browning LM, Osgood CJ, Xu XHN. In vivo imaging of transport and biocompatibility of single silver nanoparticles in early development of zebrafish embryos. *ACS Nano* 2007;1(2):133–143. [PubMed: 19122772]
34. Zhu, XS.; Zhu, L.; Duan, ZH.; Qi, RQ.; Li, Y.; Lang, YP. Comparative toxicity of several metal oxide nanoparticle aqueous suspensions to Zebrafish (*Danio rerio*) early developmental stage, 2008. Taylor & Francis Inc; 2008. p. 278-284.
35. Henry TB, Menn FM, Fleming JT, Wilgus J, Compton RN, Saylor GS. Attributing effects of aqueous C-60 nano-aggregates to tetrahydrofuran decomposition products in larval zebrafish by assessment of gene expression. *Environmental Health Perspectives* 2007;115(7):1059–1065. [PubMed: 17637923]
36. Usenko CY, Harper SL, Tanguay RL. In vivo evaluation of carbon fullerene toxicity using embryonic zebrafish. *Carbon* 2007;45(9):1891–1898. [PubMed: 18670586]
37. Wallace KN, Akhter S, Smith EM, Lorent K, Pack M. Intestinal growth and differentiation in zebrafish. *Mechanisms of Development* 2005;122(2):157–173. [PubMed: 15652704]
38. Wallace KN, Pack M. Unique and conserved aspects of gut development in zebrafish. *Developmental Biology* 2003;255(1):12–29. [PubMed: 12618131]
39. Choi HS, Liu W, Misra P, Tanaka E, Zimmer JP, Ipe BI, Bawendi MG, Frangioni JV. Renal clearance of quantum dots. *Nature Biotechnology* 2007;25(10):1165–1170.
40. Lacerda L, Herrero MA, Venner K, Bianco A, Prato M, Kostarelos K. Carbon-nanotube shape and individualization critical for renal excretion. *Small* 2008;4(8):1130–1132. [PubMed: 18666166]
41. Asharani PV, Wu YL, Gong ZY, Valiyaveetil S. Toxicity of silver nanoparticles in zebrafish models. *Nanotechnology* 2008;19(25)

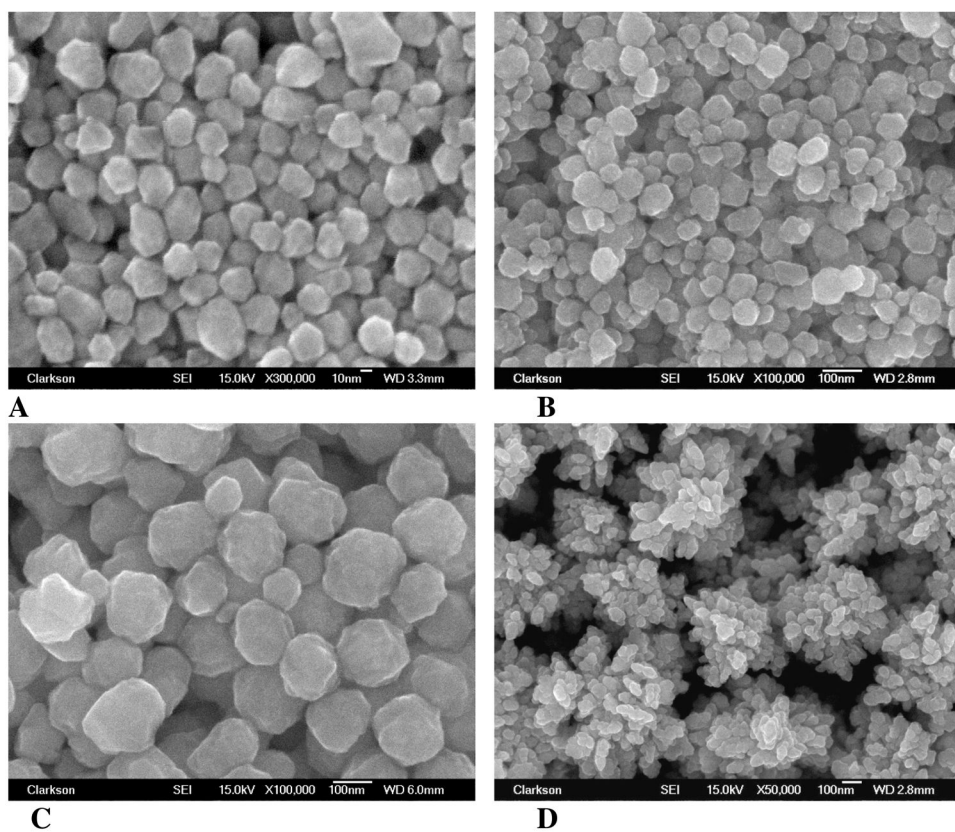


Figure 1. FE-SEM images of Ni NPs with an average particle diameter of 30 nm (A), 60 nm (B), 100 nm (C), and dendritic structures with aggregated 60 nm entities (D).

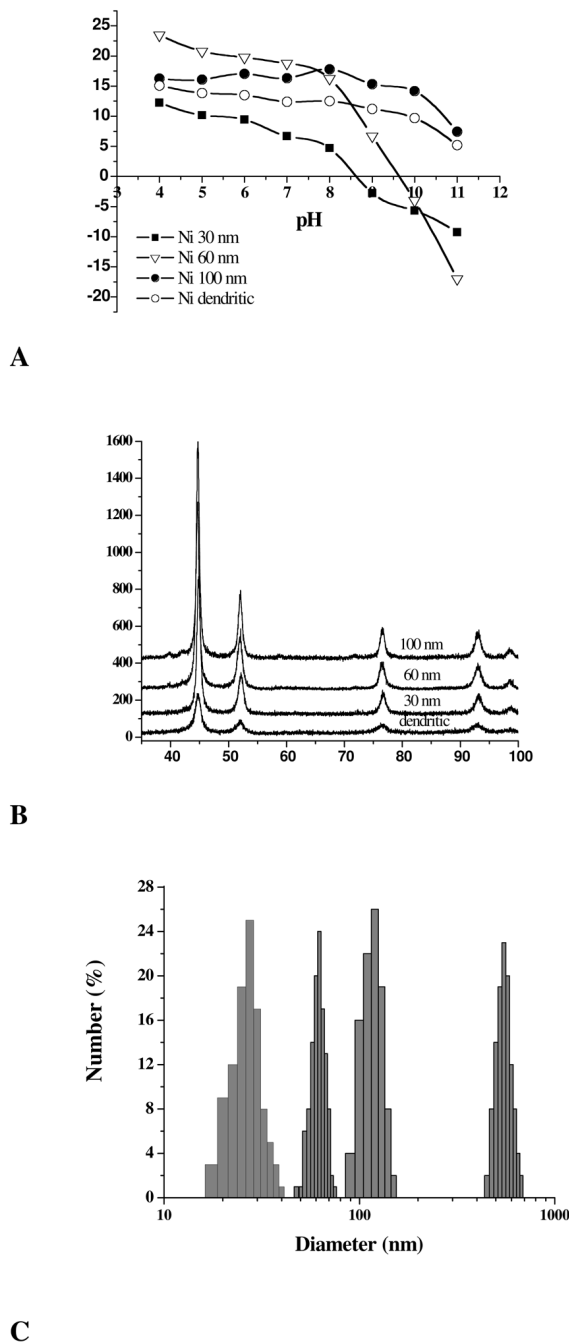


Figure 2. XRD patterns (A), zeta-potential analysis as a function of pH (B) and Particle size distribution (PSD) calculated from PSD was calculated from dynamic light scattering. PSD for the dendritic structure was estimated from field emission-scanning electron microscopy (FESEM) images from average values of 100 particles (C). Median d_{50} values as calculated from the PSD analysis are: 28, 63, 112 nm for 30, 60 and 100 nm particles and 540 nm for dendritic particles.

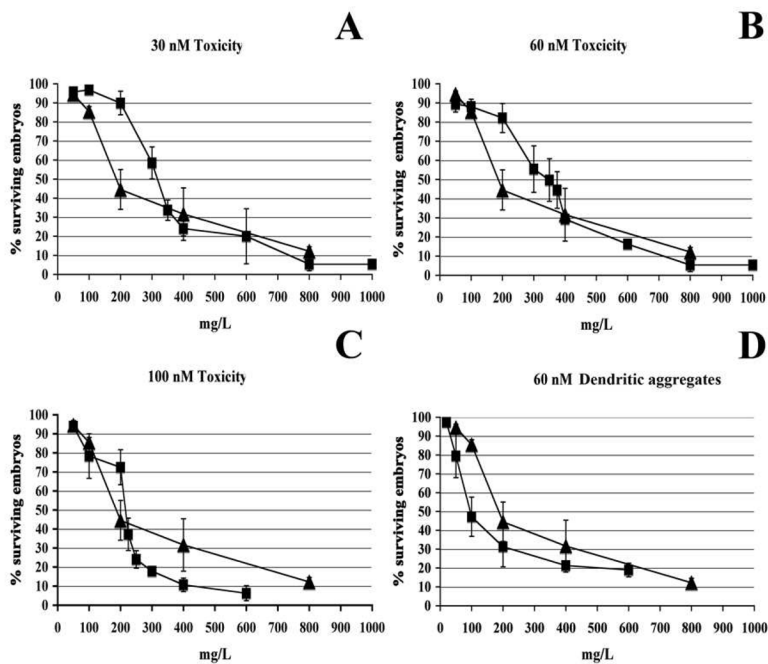


Figure 3. Concentration-response curves for toxicity of different size and shape nickel nanoparticles Toxicity of each nickel NPs (square) is compared to equivalent concentrations of soluble nickel (triangle). Each trial consist of 25 embryos and values are presented as the mean \pm standard error (n= 3–6).

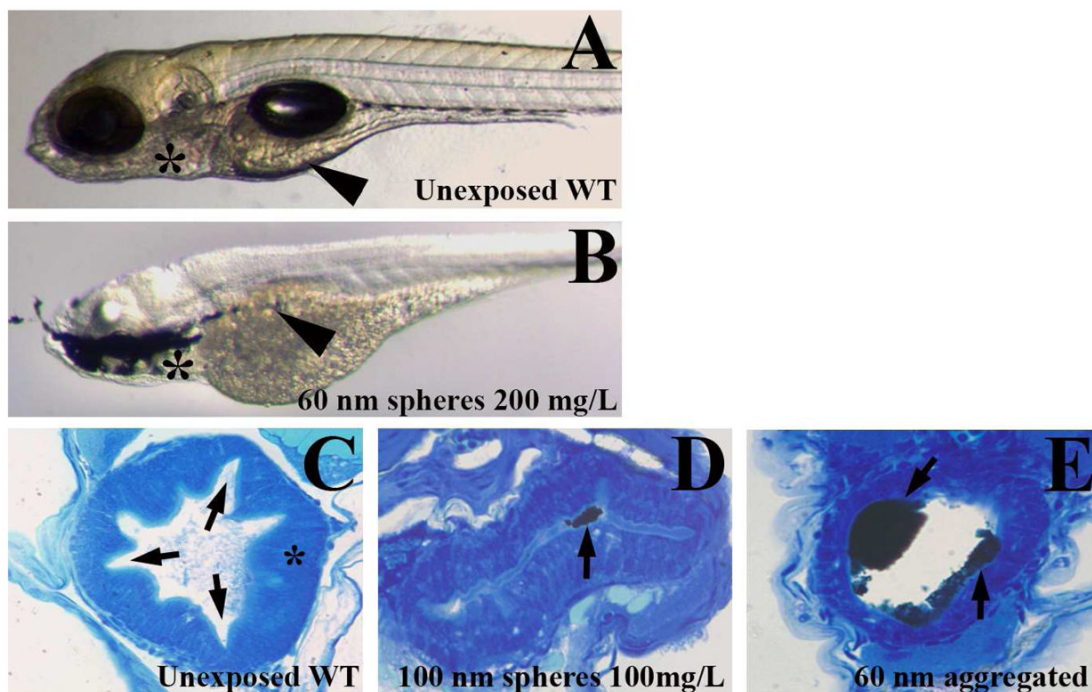


Figure 4. Nickel nanoparticles accumulate within the lumen of the digestive system to different levels

Unexposed wild type embryos in whole mount (A arrowhead) and in cross section (C arrows) have highly folded anterior intestines and columnar epithelial cells (C asterisks). Ni NPs can aggregate within the pharynx and intestine to high enough levels to be observed in whole mount (B pharynx asterisks and intestine arrowhead, 60 nm Ni NPs). Intestinal sections show the variation in Ni NP accumulation between exposures. Often small accumulations of Ni NP are present (arrow in D, 100 nm Ni NPs) while in some cases a much larger quantity will aggregate (arrows in E, dendritic aggregates of 60 nm).

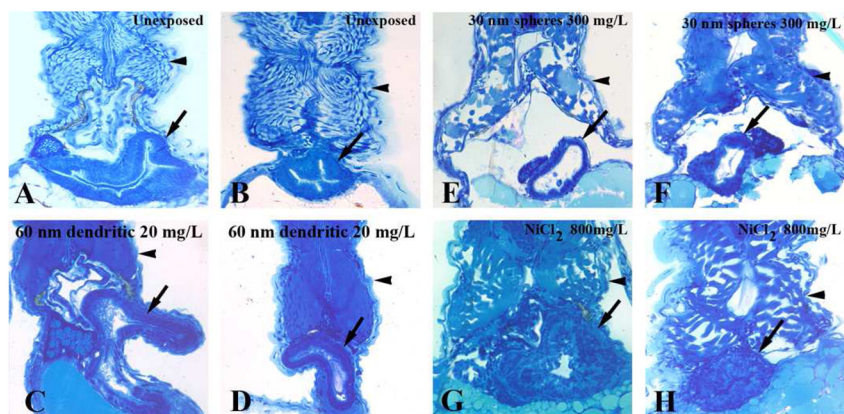


Figure 5. Nanoparticle nickel and soluble nickel generate different defects in zebrafish embryos
 Cross-sections of unexposed embryo intestines have columnar epithelial cells with multiple folds (anterior- arrow in A and posterior- arrow in B). Skeletal muscle throughout the trunk is organized and continuous (arrowhead A and B). Exposure of nickel nanoparticles to concentrations around the LD10 results in thin intestines with cuboidal epithelial cells (anterior- arrow in C and posterior- arrow in D, dendritic aggregates) and unaffected skeletal muscle (anterior- arrowhead in C and posterior- arrowhead in D). Embryos exposed to NPs at concentrations around the LD50 still have thin walled intestines (anterior- arrow in E and posterior- arrow in F, 30 nm Ni NPs) but now skeletal muscle fibers have become separated throughout the trunk (anterior- arrowhead in E and posterior- arrowhead in F). Embryos exposed to soluble nickel have columnar epithelial cells and multiple folds (anterior- arrow in G and posterior- arrow in H) in the intestine even at concentrations well over the LD50. Separated skeletal muscles are first observed at concentrations in the 800 mg/L range (anterior- arrowhead in G and posterior- arrowhead in H).

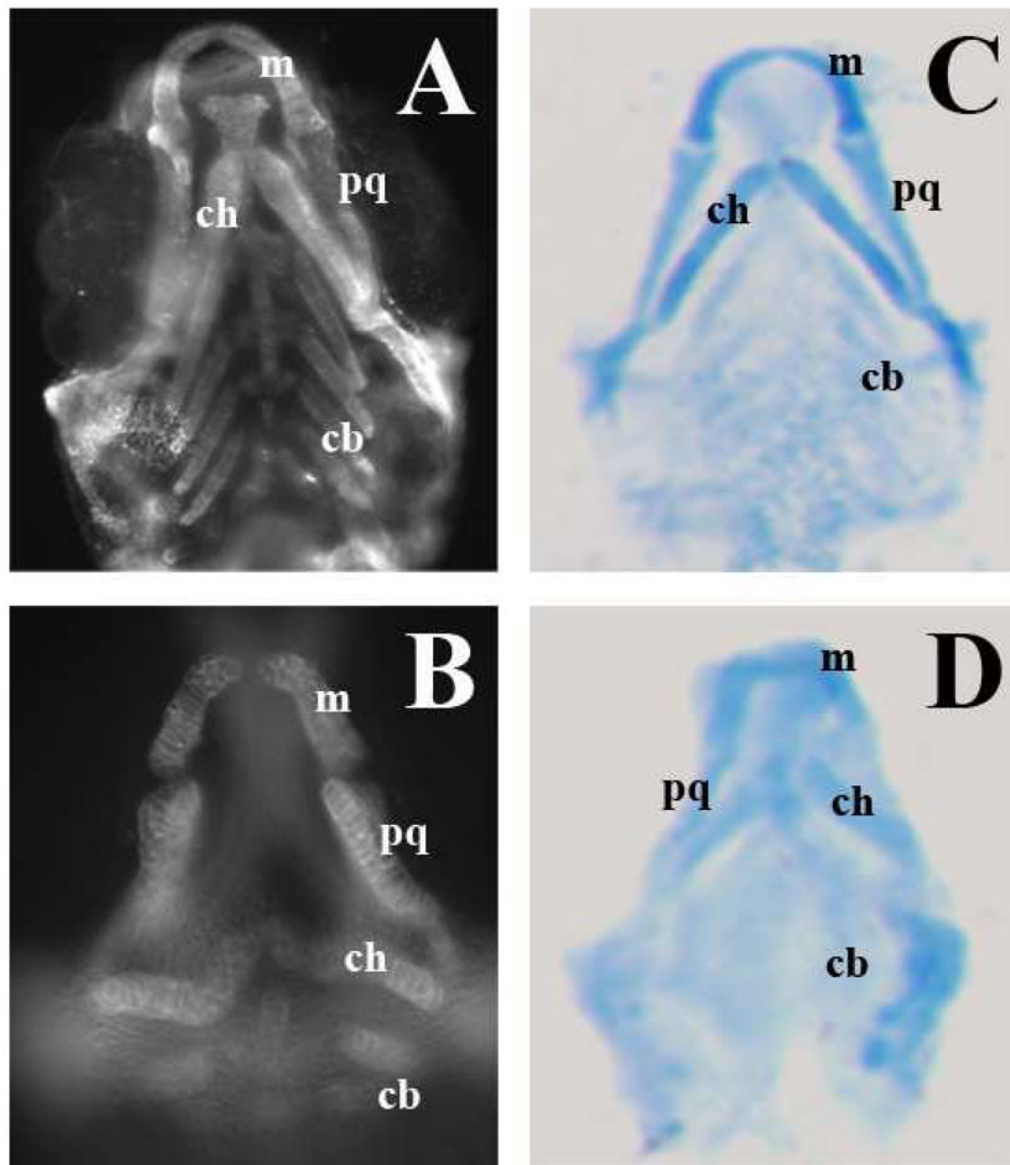


Figure 6. Nickel nanoparticle generates jaw cartilage defects around LD50 concentrations

Wild type whole mounts of collagen immunohistochemistry (A) and alcian blue staining (C) show the normal distribution of ventral jaw cartilages. The spacing of Meckel's and the ceratohyal become affected while ceratobranchials have less staining and become less organized with exposure to 200 mg/L 60 nm Ni aggregated as shown by collagen (B) and alcian blue (D). m- Meckel's; ch- ceratohyal; pq- palatoquadrate; cb- ceratobranchial.

Table 1

Summary of structural, morphological and solubility studies for four types of Ni particles used in the cytotoxicity experiments.

Ni sample shape/size	SSA experimental ¹ vs theoretical ² value (m ² /g)	Particle size distribution (nm) ⁴	Solubility as determined by ICP-MS analysis (mg/L) (± SD)
Spherical/100 nm	8.53/6.75	112	15.6 (± 0.5)
Spherical/60 nm	16.38/11.20	63	23.13 (± 2.11)
Spherical/30 nm	21.77/22.40	28	23.38 (± 1.12)
Dendritic/aggregated 60 nm entities	~ 14(±20%) ³ /-	540 ⁵	24.48 (± 0.76)

SSA - specific size area.

¹ Experimental SSA- BET values.

² Theoretical SSA calculated using the formula: $SSA (m^2/g) = 6/(\rho_{Ni} \times d)$ where: ρ_{Ni} = specific gravity of Ni, and d = diameter, assuming that Ni particles are spherical.

³ Estimated value based on the area of the individual 60 nm entities. SD - standard deviation from three replicates.

⁴ PSD was calculated from dynamic light scattering.

⁵ The PSD for dendritic structure was estimated from field emission-scanning electron microscopy (FESEM) images.

Table 2

Toxicity of Ni nanoparticles and soluble Ni on zebrafish embryos in mg/L. LD10= 10% lethal concentration and LD50= median lethal concentration. Values in parentheses are 95% confidence intervals.

Nickel	LD10	LD50
30 nm Spheres	187 (143–229)	328 (299–357)
60 nm Spheres	189 (111–264)	361 (315–404)
100 nm Spheres	172 (140–188)	221 (212–231)
Dendritic particles of aggregated 60 nm spheres	21 (9–43)	115 (90–168)
Soluble nickel	63 (40–96)	221 (181–271)